ELECTROTHERMAL MODEL AND SIMULATION OF AN ELECTRIC AIRCRAFT BATTERY SYSTEM AND CURRENT STATE ASSESSMENT OF HIGH-PERFORMANCE LITHIUM CATHODE MATERIALS

Antonio Andreoli
Politecnico di Milano
Milan, Italy

Riccardo Pirrello
Leonardo SpA - Helicopters Division
Samarate, Italy

Cristina Antonioli
Leonardo SpA - Helicopters Division
Samarate, Italy

1 Abstract

This work addresses the application of lithium batteries to eVTOLs. A detailed current state assessment of five lithium-based cathode materials is presented, with a particular emphasis on new emerging materials, their limitations and strategies to improve their performance, and a focus on specific energy, specific power, and safety. A battery system is then proposed according to the energy and power requirements of a flight mission for a short regional flight. A detailed electrothermal model of the proposed battery system is then implemented in the MATLAB® and Simulink® environment and simulated to assess its performance and to understand the complex evolution of electrical and thermal quantities of the battery cells during the different flight phases. The developed model is intended to be a flexible tool which can be used to approach the design of a battery and its thermal management system. Due to its reliance on look-up tables, its implementation can be performed using readily available cells datasheet without the need of a detailed cell characterization, allowing a fast comparison between different configurations and scenarios.

2 Notation

Acronyms

EASA European Union Aviation Safety Agency

eVTOL Electric Vertical Take Off and Landing

LMFP Lithium Manganese Ferrophosphate

LMNO Lithium Manganese Nickel Oxide

LLO Lithium Layered Oxides

NCA Nickel Cobalt Aluminum

NMC Nickel Manganese Cobalt

OAT Outside Ambient Temperature

SEI Solid Electrolyte Interphase

SOC State Of Charge

3 Introduction

eVTOLs (Electric Vertical Take-Off and Landing) are a new class of aircraft designed to offer fast and flexible mobility solutions for regional air transportation. eVTOLs combine distributed electric propulsion and reduced size to enable quiet and flexible vertical take-off and landing ability. They are usually characterized by a tilt rotor design, in order to leverage both the vertical takeoff capabilities of a helicopter and the improved speed and range of a conventional fixed-wing aircraft. Several challenges must be addressed before eVTOLs become a viable transportation option. Battery technology remains the technological limiting factor. Specific energy generally limits the maximum range, while specific power generally limits takeoff weight, as a great amount of power is required to perform both lift and landing maneuvers at the beginning and end of the mission. A careful evaluation of the battery's requirements and capabilities is essential. The first part of this work provides a comprehensive review of six different cathode materials and an overview of degradation mechanisms relevant to high-performance applications. In the second part, a battery layout that can meet the mission requirements is proposed. A detailed electrothermal model of the proposed battery system is then implemented and simulated to assess its performance and to understand the complex evolution of electrical and thermal quantities of the battery cells during the different flight phases. The developed model is intended to be a flexible tool which can be used to approach the design of a battery and its thermal management system.

4 Electrochemistry of Lithium

The energy stored inside an electrochemical cell during the discharging is released according to spontaneous oxidation-reduction reaction. The essential components of a elemental cell are four: the cathode, the anode, the separator, and the electrolyte (Fig. 1). During discharge, a flow of electrons establishes as the anode is oxidized (ie, it loses electrons) and the cathode is reduced (ie, it gains electrons). The role of the electrolyte is to provide an efficient medium for transfer of positively charged Li^+ and the separator allows their passage while blocking electrons by electrically insulating the cathode from the anode. For a generic lithium-ion cell (hereinafter, Li-ion cell) with layered oxide cathode and carbon-based anode, the general reaction is described in Equation (1), while the two cathode half-reactions are described in Equation (2) and Equation (3), respectively.

Overall Reaction:

$$\mathrm{LiMO_2} + \frac{x}{y}\,\mathrm{C} \rightleftharpoons \frac{x}{y}\,\mathrm{Li}_y\mathrm{C} + \mathrm{Li}_{1-x}\mathrm{MO_2} \tag{1}$$

Cathode:

$$\mathrm{LiMO_2} \rightleftharpoons \mathrm{Li}_{1-x}\mathrm{MO_2} + x\,\mathrm{Li}^+ + x\,e^- \tag{2}$$

Anode:

$$\mathrm{C} + y\,\mathrm{Li}^+ + y\,e^- \rightleftharpoons \mathrm{Li}_y\mathrm{C} \tag{3}$$

The half-reaction of the anode (Eq. 3) describes a intercalation of Li^+ ions into the layered structure of the carbon-based graphite anode (the most common type of anode material). In other words, intercalation consists in the reversible insertion of an ion (the guest) into a framework structure (the host) by chemical or electrochemical means. The stoichiometry of the two half-reactions depends on the nature of the anode and cathode; however, all the reactions involve the intercalation of lithium ions regardless of the cathode and anode materials (Fig. 2).

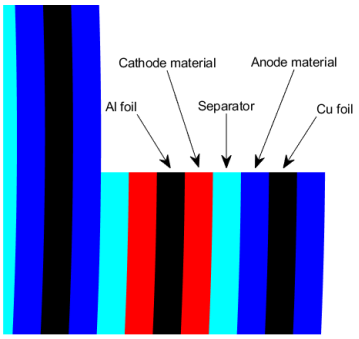

Figure 1: Detailed view of the cylindrical cell's internal structure (not in scale).

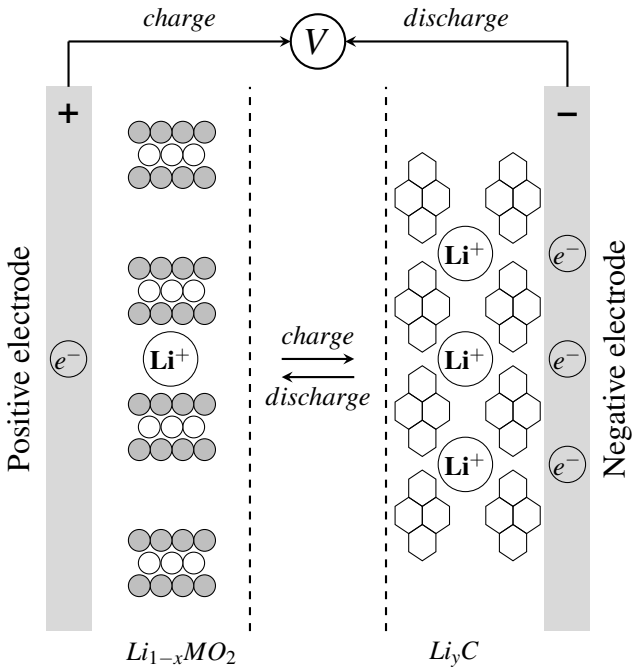

Figure 2: Schematic diagram of intercalation.

4.1 Cathode Materials

In commercially available Li-ion cells a lithiated metal oxide or lithiated metal phosphate is the active material; such materials have to satisfy multiple requirements. In order to provide high capacity, they must incorporate a large amount of lithium and high potential (vs. Li/Li^+) is needed in order to obtain high cell voltage. At the same time, in order to achieve high coulombic and energy efficiency and long cycle life, they need to reversibly exchange lithium, with minimal structural changes. Lithium based cathode materials are classified into three main different types depending on their structure: layered oxides, spinel oxides and polyanionic olivine materials. Currently, layered oxides are the best performing ones, with a good balance between energy density, safety, and longevity. Olivine materials, despite having a lower energy density, offer exceptional safety and longevity. Finally, spinel oxides are only marginally used because of their lower safety and limited longevity; nonetheless, lithium-rich spinel materials offer exceptionally high energy density (Fig. 3).

Nickel Cobalt Aluminum — NCA Lithium nickel cobalt aluminium oxides $LiNi_{0.8}Co_{0.2-x}Al_xO_2$ $(0 \leq x \leq 0.1)$ are cobalt and aluminium co-doped nickel lithium oxides. Bulk doping, which consists in the partial substitution of nickel for various elements, can significantly lower and stabilize their impedance, allowing higher voltage without compromising the cell capacity. Magnesium-doped NCAM1 cathode material exhibits a discharge capacity of $226.4\,\mathrm{mA\,h\,g^{-1}}$ in a cell voltage range of 2.5 V–4.7 V and suppressed degradation (Ref. 2). When properly enhanced, NCA materials demonstrate exceptionally high specific capacity and long cycle life. Limited thermal stability, high cost, and capacity fade at high

temperatures are the main aspects that hamper the use of this cathode technology.

Nickel Manganese Cobalt — NMC Lithium manganese nickel cobalt oxide $LiNi_{1-x-y}Co_xMn_yO_2$ is a layered compound material made of three different mixed metal oxides ($LiNiO_2$, $LiCoO_2$ and $LiMnO_2$). Depending on the proportions of the different oxides, different compounds with specific properties can be obtained, enhancing the capacity, improving thermal stability and capacity retention. The typical specific capacity of lithium nickel manganese cobalt cathodes is $150\,\mathrm{mA\,h\,g^{-1}}$ in a cell operating voltage range of 2.5 V–4.2 V. Increasing the voltage range to 3.5 V–5 V allows to obtain $200\,\mathrm{mA\,h\,g^{-1}}$ with little capacity fading (Ref. 4). NMC materials strike a balance between performances, lifespan and reliability. With a specific capacity essentially equivalent to the materials with elevated cobalt content, with the added advantages of lower cobalt content, improved safety, and longer cycle life.

Lithium Layered Oxides — LLO Lithium layered oxides $Li[M_xLi_{1/3-2x/3}Mn_{2/3-x/3}]O_2$ $(0 \leq x \leq 1)$ with $M = Mn$, Co, Ni or their mixture, are cobalt free materials composed of two layered phases. They are characterized by a long oxygen activation plateau caused by the participation of oxygen atoms in the electrochemical reactions; this activation provides additional specific capacity to the cathode material. Oxygen participates in both a reversible and an irreversible process. Reversible participation determines a hysteretic behavior in the form of a plateau around 4.5 V. The irreversible participation determines a rapid irreversible fading of the capacity in the first few cycles. The typical specific capacity is of $200\,\mathrm{mA\,h\,g^{-1}}$–$240\,\mathrm{mA\,h\,g^{-1}}$ in a cell operating voltage range of 2 V–5 V, with a marked negative correlation on the discharge rate (Ref. 3). Although very promising, the high reactivity between cell components leads to voltage fading, short cycle life and accelerated degradation at high temperatures.

Lithium Manganese Ferrophosphate — LMFP Olivine compounds have a high theoretical capacity, low cost, ease of synthesis, safe handling and operation, environmental benignity and exceptional stability up to extremely high temperatures when used with common organic electrolyte systems. Among them, lithium ferrophosphate stands out for its superior cycling stability and lithium manganese phosphate for its high operating voltage. To leverage the advantages of both, lithium manganese ferrophosphate $LiMn_xFe_{1-x}PO_4$ is usually adopted as a cathode material with exceptional cycling capabilities. Its typical specific capacity is of $150\,\mathrm{mA\,h\,g^{-1}}$ in a cell operating voltage range of 2.5 V–3.5 V. The main disadvantage of LMFP materials are their low intrinsic electronic conductivity which needs to be addressed combining four main approaches: bulk doping, coating, multiscale particle regulation, and microscopic morphology design (Ref. 6). This results in a lowered specific capacity.

Lithium Manganese Nickel Oxide — LMNO The high voltage, cobalt-free spinel material $LiMn_2O_4$ is characterized by a very high energy density thanks to the high operating voltage. To prevent capacity fading, it is possible to stabilize the spinel structure by substituting manganese ions for metal ones. The resulting $LiMn_{2-x}MO_4$ material (with $M = Cr, Ni, Co$ and Cu) exhibits an outstanding operating voltage of nearly 5 V and a capacity of $100\,\mathrm{mA\,h\,g^{-1}}$–$150\,\mathrm{mA\,h\,g^{-1}}$. Like for lithium layered oxides materials, lithium nickel manganese oxides charging curves are stepwise, being characterized by two plateaus. The first around 4 V and the second near 4.7 V (Ref. 5) due to the reversible participation of the manganese and the substituting metals, respectively, in the electrochemical reactions. Bulk doping is fundamental to achieve an acceptable structural stability; adequate proportions of binder and carbon materials are essential to avoid premature cell degradation at high temperature. Challenging high-voltage operating conditions and side chemical reactions limit practical applications of this material, and require a careful evaluation of the possible side reactions between different components of the cell.

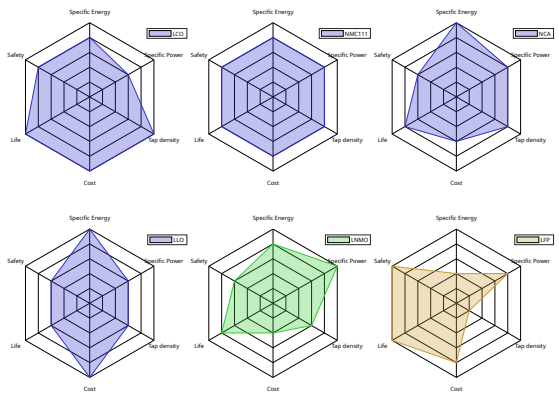

Figure 3: Comparison between different cathode materials.

4.2 Degradation Mechanisms

The effects of the many degradation mechanisms can be summarized in three different degradation modes: loss of lithium inventory, loss of active cathode material, and loss of active anode material. The primary effect of these degradation mechanisms is an increase in internal resistance. Consequently, an increase in the internal resistance leads to a reduced useful cell capacity since, for a higher internal resistance, the lower cut-off voltage is reached sooner. The available output energy is also reduced because of the increased losses. The causes of degradation are usually related to temperature, state of charge (SOC), operating voltage, and current. High working temperatures essentially catalyze the degradation reactions that occur between the cell components. However, the power capabilities of the cell, especially during charging, could be temporarily enhanced as a result of the positive effect of temperature on electrolyte conductivity, intercalation kinetics, and solid-state diffusivity. High V_{cell}/SOC_{cell} can cause lithium plating due to the accumulation of lithium on the anode side. Dually, V_{cell}/SOC_{cell} can deplete the active

cathode material of lithium ions and reduce the thickness of the SEI layer. The value of the current load can greatly influence the degradation rate of the cell and is associated with the highest number of degradation mechanisms among all the degradation causes. The main cause of capacity loss degradation for high current charging is lithium plating (Ref. 1).

5 Battery Pack Layout

For eVTOL applications, the choice for the best cell technology currently comes down mainly to two types of cathode materials: NMC and NCA. Cylindrical and pouch cells are currently the most popular form factors for high-performance NMC and NCA cells. The cell selected for the battery system is the MOLICEL INR-21700 P45B. The cylindrical cell has dimensions of 21 mm diameter and 70 mm in length. This form factor provides an optimal balance between energy density and thermal management capabilities. The cathode active material is Nickel Manganese Cobalt (NMC) based, and the anode is graphite-based. This results in a typical capacity of 4500 mA h corresponding to 16.2 W h of energy, equivalent to 242 W h kg^{-1} or 643 W h L^{-1}. This cell is characterized by an exceptionally low internal resistance, designed for high discharge rates. The cell can sustain continuous discharge rates up to 10C and charge rates up to 3C in a temperature range of -40 to 60 °C and 0 to 60 °C respectively. The cell operates in a voltage range of 2.5 V–4.3 V, with nominal voltage of 3.6 V. The sizing of the battery system is determined by the energy requirements of the flight mission. A mission profile with five different flight phases is considered. The proposed battery *pack* (Fig. 4) consists of two parallel-connected *module assemblies*, each comprising 6 series-connected *modules*. Each module consists of 37 series-connected *parallel assemblies*, with 4 parallel-connected *cells* for each parallel assembly.

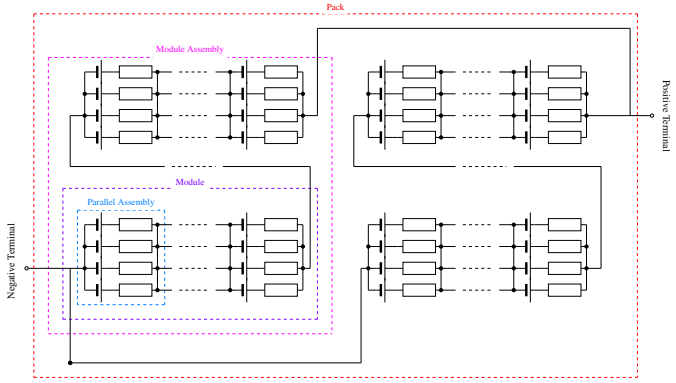

Figure 4: Proposed layout.

6 Battery Pack Electrothermal Model

Although it cannot describe fast electrical transients, the fidelity of the model is considered adequate for the evolution of its quantities over the simulated time intervals.

6.1 Cell Model

Because the simulation is focused on thermal dynamics, the cell is modeled with a series-equivalent parametrized circuit. This model does not require any detailed cell characterization and is computationally efficient. The model parameters, derived from the cell datasheet, are implemented with the use of look-up tables and linear interpolation. Accordingly, the voltage v at the cell terminals depends on the state of charge, temperature and on the flowing current. In this model, the resistor R_{int} accounts for the total internal resistance and is dependent on both the state of charge and the temperature (Fig. 5). The open circuit voltage (OCV) accounts for the potential difference of the electrochemical reactions. Its value strongly depends on the cell state of charge (SOC) (Fig. 6). Therefore, the cell output voltage V depends both on the state of charge and temperature and, because the voltage drop on the internal resistance is proportional to the load current, the voltage at the terminals is also dependent on the flowing current.

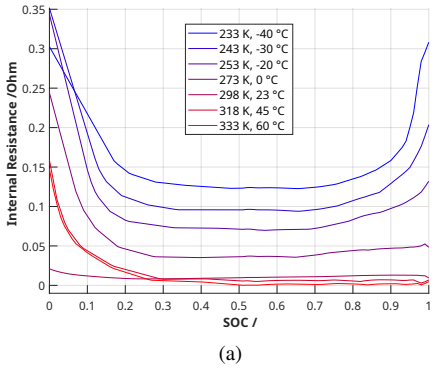

(a)

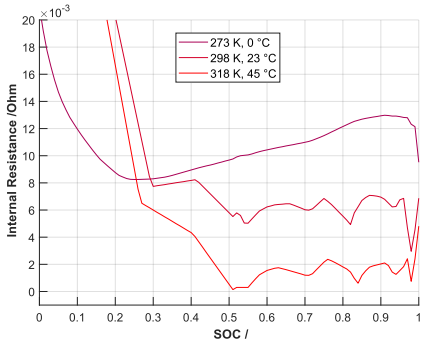

(b)

Figure 5: Resistance values as a function of the temperature and state of charge.

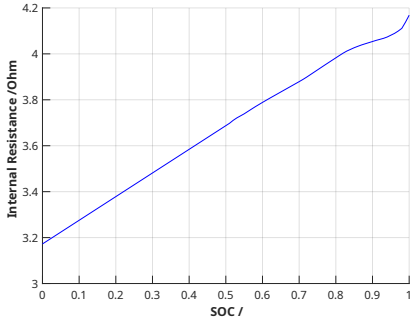

Figure 6: Open circuit voltage as a function of the SOC.

The discharging current is often expressed as a function of the C_{rate}, a characteristic quantity of the cell, defined as the discharging current over the nominal capacity:

$$C_{rate} = \frac{I_{disch}\ [A]}{q_{nom}\ [Ah]} \tag{4}$$

According to the model, the state of charge of the cell at a given instant t' can be defined as:

$$SOC(t') = SOC_{t_0} - \frac{1}{q_{\text{nom}}} \int_0^t i(t)\, dt \tag{5}$$

and the voltage at the cell terminals as:

$$v(SOC,T,t) = OCV(SOC) - R(SOC,T)i(t) \tag{6}$$

The adopted predefined model is based on the MOLICEL INR-21700 P45B datasheet data. Specifically, the parameters $OCV(SOC,T)$ and $R_{int}(SOC,T)$ are tabulated for every 1% interval of SOC for a discharge rate of $1C$ and for several different temperature values ($T = -40\,^{\circ}\text{C}$, $-30\,^{\circ}\text{C}$, $-20\,^{\circ}\text{C}$, $0\,^{\circ}\text{C}$, $23\,^{\circ}\text{C}$, $45\,^{\circ}\text{C}$ and $60\,^{\circ}\text{C}$). When the temperature falls between tabulated values, the corresponding parameter is obtained via linear interpolation.
The comparison of the simulated characteristic with the original datasheet characteristic is shown in Fig. 7. It can be seen that the accuracy of the plot is lower for both lower and higher SOC values. Because we assume a $SOC = 95\,\%$–$20\,\%$ operating interval, the model fidelity is considered adequate.

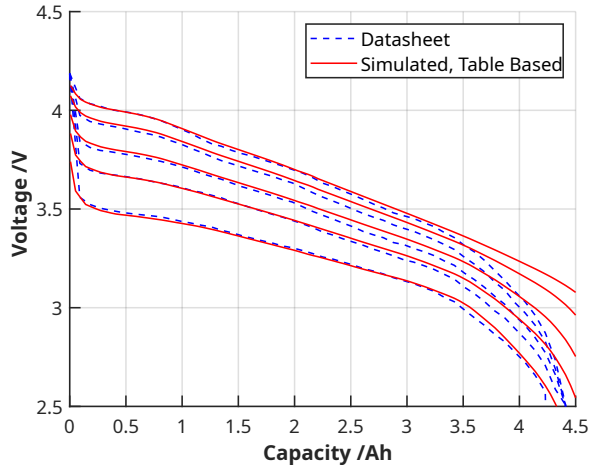

Figure 7: Simulated discharging characteristics compared with original datasheet values.

The cell electrothermal model is described using a lumped parameters model, consisting of a heat source that describes ohmic heating and a thermal capacity, that represents the cell thermal mass (Fig. 8).

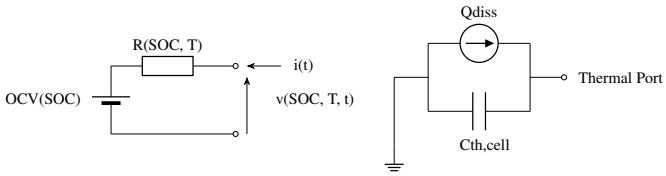

Figure 8: Cell electrical and electrothermal model.

6.2 Cells Thermal Interaction

Thermal resistance quantifies the material's ability to oppose heat transfer. Heat exchange between different cells is modeled with a thermal resistance (Fig. 9) that models conductive heat transfer. Convective heat transfer is ignored due to the small gap between adjacent cells. Because of the operating temperature range of the cells, radiation heat transfer is also negligible. Nonetheless, radiation could be the predominant heat transfer mode in case of thermal runway. Because the definition of thermal runway insulation requirements is not the aim of this work, the simulated model will not consider the presence of any interface material but air. Accordingly, the thermal resistance between adjacent cells can be found as:

$$R_{\text{th}} = \frac{\Delta x}{A \cdot k} \quad \left[\frac{\text{K}}{\text{W}}\right] \tag{7}$$

where:

- Δx is the thickness (measured on a path parallel to the heat flow).
- A is the cross-sectional area perpendicular to the path of heat flow.
- k is the thermal conductivity of air, assumed constant.

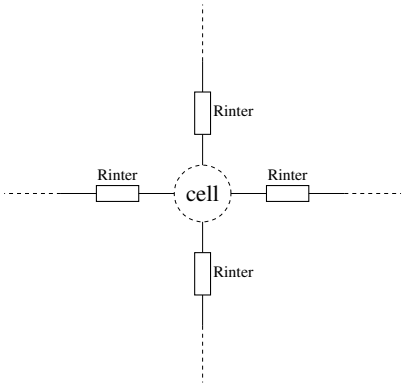

Figure 9: Thermal resistance between cells.

6.3 Cells at the boundary

Cells at the sides of the battery pack are exposed to both the surrounding cells and to ambient temperature through the battery pack enclosure. To take into account the thermal interaction with the ambient, the thermal masses of the cells at the boundary are connected to a thermal resistor (Fig. 10). The pack case is assumed at a steady temperature equal to the external ambient temperature. Because the cell surface exposed to the case is approximated to double the surface area exposed between cells and the distance between the cell and the case is equal to the inter cell resistance, the assumed value of the thermal resistance can be approximated to $R_{ext} = \frac{1}{2}Rinter$. Although each cell interfaces with the external ambient via the positive electrode, the interaction is neglected because of the reduced surface area exposed.

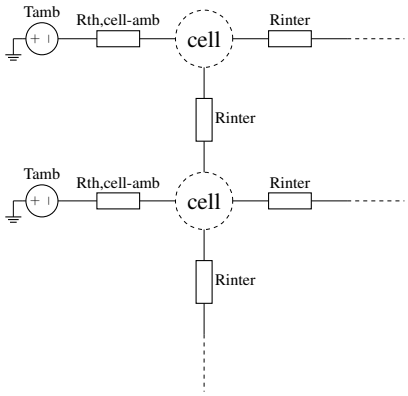

Figure 10: Thermal resistance between cells and boundary.

6.4 Cooling Plate Thermal Model

The cell thermal network interacts with the cooling plate thermal network via the bottom surface of the negative terminal of the cells. Each capacity represents the thermal mass of one cooling plate subregion. The cooling fluid is represented with an equivalent temperature source. A thermal resistor represents thermal resistance between the flowing fluid and the subregion. Every subregion can exchange heat with the surrounding ones via a thermal resistor (Fig. 11).

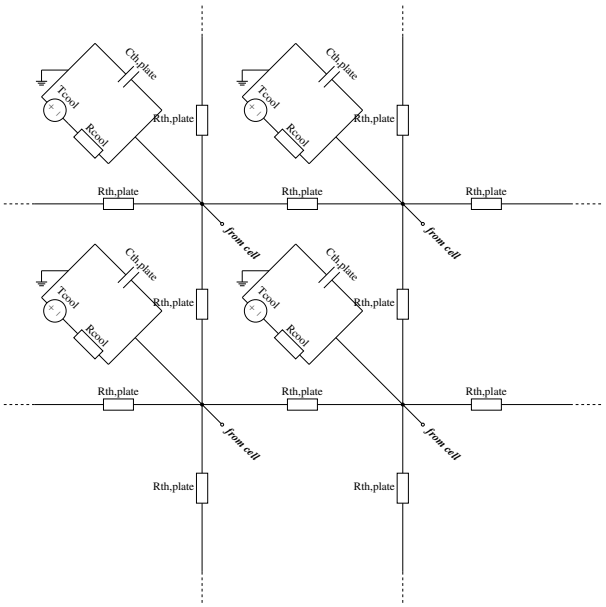

Figure 11: Cooling plate thermal network model.

6.5 Complete Model

The resulting electrothermal model of the battery system takes into account both the electrical dissipative phenomena and the thermal interaction between the cells. The interaction with the external environment is modeled as a series equivalent circuit, where the voltage source represents the external ambient temperature, and the resistor represents the thermal resistance between the cells on the edge of the battery and the external environment. A node connects each cell to the corresponding subregion area of the cooling plate (Fig. 12).

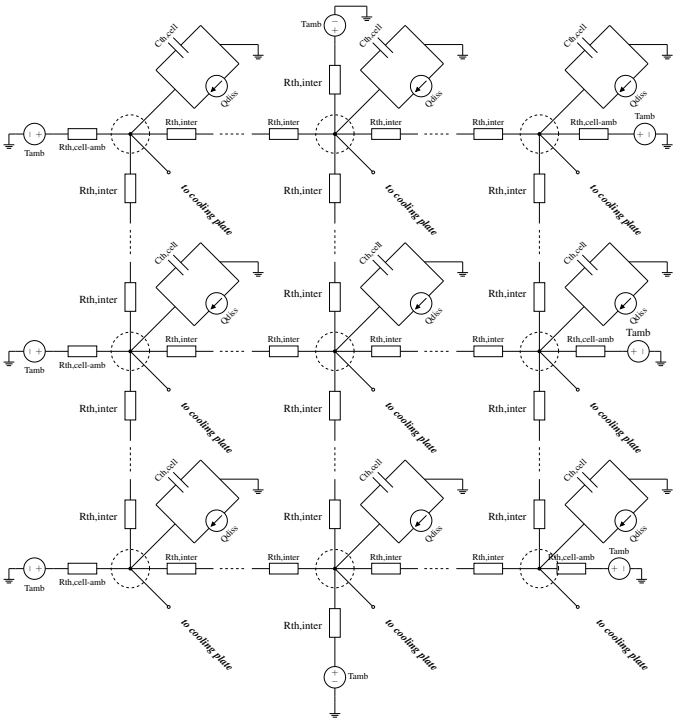

Figure 12: Battery system thermal network model.

7 Simulation

7.1 Environmental Conditions

Current existing requirements for aircraft certification are very demanding in terms of both Outside Ambient Temperature (OAT) and avionics bay temperature ranges for which the aircraft operation must be ensured. The first refers to the temperature of the air around an aircraft, unaffected by the passage of the aircraft through it. The second to the temperature of the air inside the compartment that houses avionics and other electronic equipment including batteries. The European Union Aviation Safety Agency (EASA) ongoing Special Condition VTOL (SC-VTOL) standards do not specify a universal maximum operating temperature for eVTOL aircraft. Instead, EASA requires manufacturers to define and demonstrate the performance and safety of their aircraft in a range of environmental conditions, including high temperatures (Ref. 7). Therefore, the worst-case scenario currently required for certification is adopted. Specifically, the maximum temperature value $T_{OAT,max} = ISA + 35 = 323\,\mathrm{K}$ (50 °C) and the maximum bay temperature value $T_{bay,max} = 343\,\mathrm{K}$ (70 °C). The battery system is supposed to be conditioned from ground by an infrastructure at a temperature $\sim 20\,\mathrm{K}$ lower than the external temperature. The ambient temperature is assumed to be constant during the mission due of the limited cruise altitude of the eVTOL. Moreover, it is assumed that the constant flow rate pump is activated only when the temperature of the hottest cell reaches the initial temperature of the coolant. The thermal management system is assumed ideal and at a steady temperature.

7.2 Simulation Results

To evaluate the performance of the module assembly in detail, only two modules are considered. A module on the edge of the module assembly and a module located in the middle. The first module, located on the edge of the battery pack, is exposed to the external temperature of the bay in which the battery pack is placed. The second module, located in the middle of the battery pack, is only partially exposed, with the vast majority of its surface surrounded by the cells of the two adjacent modules. The evolution of cell voltages, cell temperature, and cell currents is then considered.
The proposed battery system is simulated and a detailed analysis of the evolution of its quantities during each flight phase of the flight mission is performed. The simulation results confirm that the proposed layout satisfies the mission requirements. The battery capacity meets the mission requirements, retaining $\sim 30\,\%$ of excess capacity (Fig. 13).

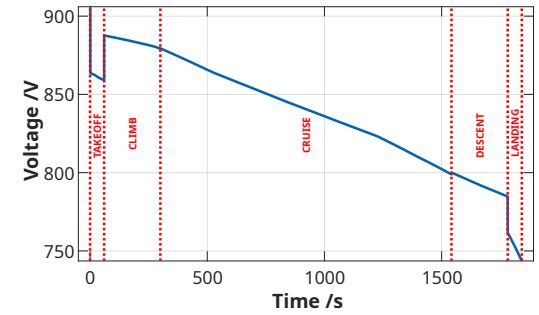

(a) Battery voltage evolution

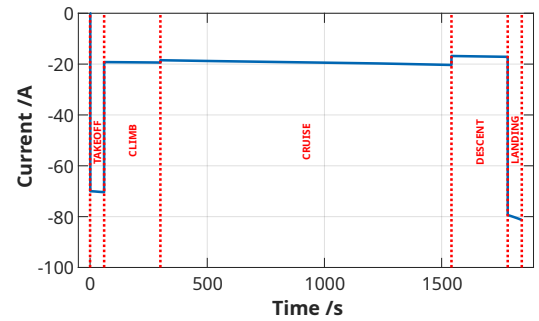

(b) Battery current evolution

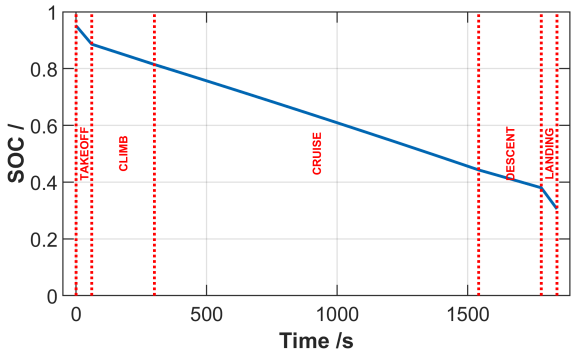

(c) Battery state of charge (SOC) evolution during the flight mission.

Figure 13: Battery voltage (a), current (b), and state of charge (c).

A detailed analysis of each flight phase of the mission profile is then performed. The values of cells temperature, current, voltage, and state of charge (*SOC*) of two modules in different positions inside the battery are illustrated to understand the complex evolution of the system quantities due to electrothermal interactions. From the results emerges a strong dependence of the cells temperature evolution (Fig. 14) on their discharge current (Fig. 15), especially during takeoff and landing. Cells at the edge of the battery system, exposed to the high temperature of the compartment, discharge faster during these power-demanding phases. This strong influence of temperature on current evolves in a complex mutual interaction between the electrical and thermal quantities. During takeoff, the temperature predominantly influences current, with minimal reciprocal effect; during climb the onset of an oscillating behavior is observed in the form of a inversion around the

mean value. The discharge current of hotter cells on the external side of the edge module suddenly lowers, vice versa for the colder cells. The inversion between hotter and colder cells repeats several times during the cruise phase (Fig. 16) and can only be explained by considering the system as a complex interacting electrothermal network. By analyzing the results near the inversion instant, it is found that the cells voltage is virtually constant because of the parallel connection between cells of the same module assembly. Therefore, the cells current inversion can be seen as a reaction of currents to the action of change in internal resistance due to the temperature variation. Therefore, the oscillating behavior of discharge current around the mean value describes the mutual influence between cell discharge current (and cell internal resistance) and cell temperature.

The temperature increases monotonically during the mission, with a speed to a certain extent proportional to the power of the different flight phases. As expected, the fastest temperature increase happens during the takeoff and the landing phases, when the required power is at its peak. Near the end of the cruise phase, the pump is activated; this causes a change in the temperature growth speed during the remaining part of the mission. At the end of the mission, during the landing phase, the cell temperatures increase as rapidly as during takeoff, although this time more uniformly. The striped nature of the plot reveals the position of the cells relative to the battery edge and the coolant inlet (Fig. 17).

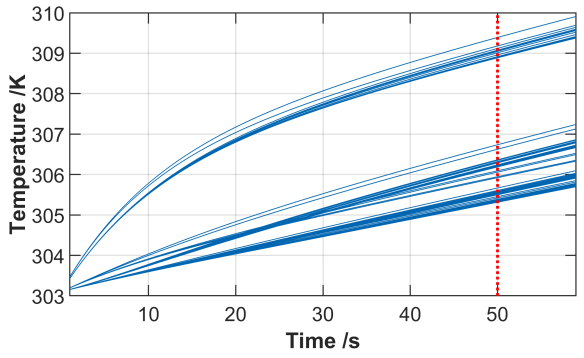

(a)

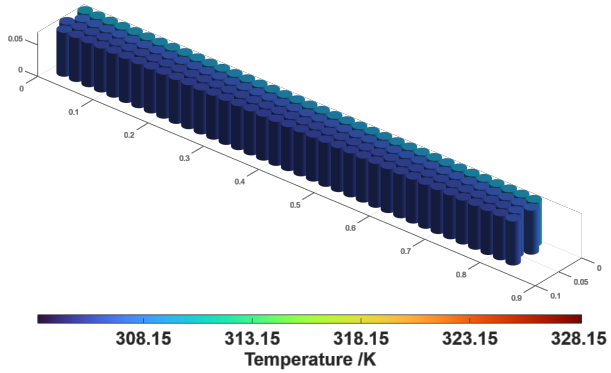

(b) edge, $t = 55s$.

Figure 14: Cells temperature evolution during takeoff, edge module (a,b).

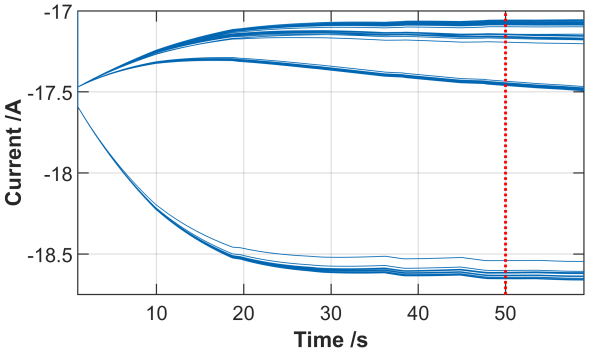

(a)

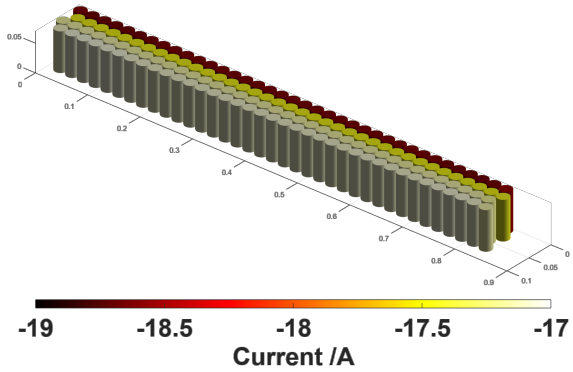

(b) $t = 50s$

Figure 15: Cells current evolution during takeoff, edge module (c,d).

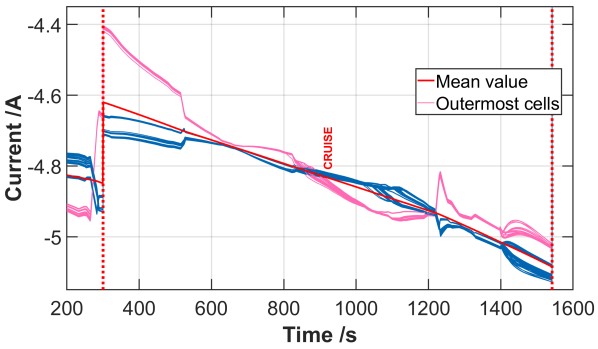

Figure 16: Oscillation of the cells discharge current around the mean value during cruise.

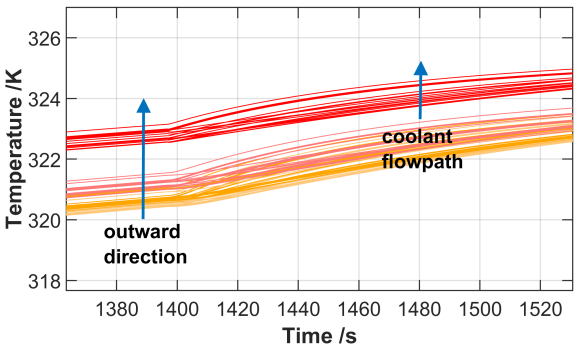

(a)

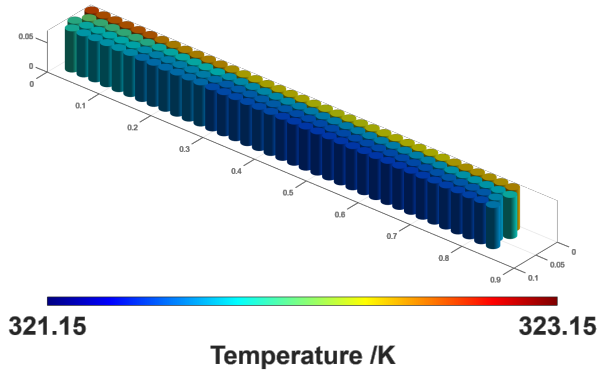

(b) $t = 1440s$

Figure 17: Edge module cells temperature during cruise.

8 Conclusions

This work is an evaluation of the applications of lithium batteries to electric vertical takeoff and landing aircraft (eVTOLs).
In the first part, a detailed review of the current state of six lithium-based cathode materials is presented, with a particular emphasis on two new emerging materials, their limitations and strategies to improve their capabilities. To select the best material for aviation applications, three main factors were considered: specific energy, specific power, and safety.

1. Among these materials, only four materials are commercially available, namely lithium nickel cobalt aluminium oxides (NCA), lithium cobalt oxide (LCO), lithium manganese nickel cobalt oxide (NMC), and lithium manganese ferrophosphate (LMFP).

2. For aircraft applications, NMC cathode materials are best-suited because of the balance between specific energy, specific power and safety.

3. NCA materials, when properly enhanced, demonstrate exceptionally high specific energy and long cycle life. Limited thermal stability and capacity fade at high temperature are the two main drawbacks of this technology.

4. LMFP materials have a high theoretical capacity, exceptional stability up to extreme temperatures, and exceptional cycle life but suffer from low intrinsic electronic conductivity.

5. Lithium layered oxides (LLO) and lithium manganese nickel oxides (LMNO) are the remaining two explored materials of lower technological maturity. Although very promising because of the highest specific energy among all six materials, they still suffer from accelerated degradation and limited thermal stability, especially LLOs.

In the second part, a battery system layout is proposed according to given eVTOL flight mission requirements and the battery system modeled with a detailed electrothermal model.

1. It is found that the proposed solution meet both energy and power requirements, while thermal requirements are met provided that the battery system is pre-cooled from ground when Outside Ambient Temperature (OAT) is in the upper limit of the adopted certification requirements.

2. From the results emerges a strong dependence of the cells temperature evolution on their discharge current.

3. At the end of the climb phase, when the required power abruptly lowers, there is a first sudden inversion in the cells discharge current magnitudes around their average value. This inversion between hotter and colder cells repeats several times during the mission. It can be noticed that, despite these sudden inversions, the cell currents tend to converge around an average value. The cells current inversion can be seen as a reaction of currents to the action of change in internal resistance due to the temperature variation.

In conclusion, the developed electrothermal model is intended to be a flexible tool which can be used when approaching the simulation of a battery and its thermal management system. Due to its reliance on look-up tables, it can be implemented using readily available data without the need of a detailed cell characterization. This results in a both time-efficient and computationally efficient approach, though this efficiency may comes at the expense of reduced accuracy in capturing fast electrical transients. Regardless, the model allows for a detailed evaluation of both electrical and thermal quantities evolution of the battery system during the different flight mission phases, allowing a rapid comparison between different designs and scenarios.

Author contact
Antonio Andreoli, antonio1.andreoli@mail.polimi.it
Riccardo Pirrello, riccardo.pirrello@leonardo.com
Cristina Antonioli, cristina.antonioli@leonardo.com

9 Acknowledgments

This work was developed in conjunction with Leonardo, Helicopters Division and Politecnico di Milano, as a part of a master thesis project. The author wants to express his appreciation to the Leonardo Helicopters Electrical Systems team, the Politecnico di Milano Department of Electrical Engineering and to all those who contributed to its development.

10 References

1. C. R. Birkl, M. R. Roberts, E. McTurk, P. G. Bruce, and D. A. Howey, "Degradation diagnostics for lithium ion cells," *Journal of Power Sources*, vol. 341, pp. 373–386, 2017.

2. B. Huang, X. Li, Z. Wang, H. Guo, and X. Xiong, "Synthesis of Mg-doped $LiNi_{0.8}Co_{0.15}Al_{0.05}O_2$ oxide and its electrochemical behavior in high-voltage lithium-ion batteries," *Ceramics International*, vol. 40, no. 8, Part B, pp. 13223–13230, 2014.

3. S. Hy, H. Liu, M. Zhang, D. Qian, B.-J. Hwang, and Y. S. Meng, "Performance and design considerations for lithium excess layered oxide positive electrode materials for lithium ion batteries," *Energy & Environmental Science*, vol. 9, no. 6, pp. 1931–1954, 2016.

4. T. Ohzuku and Y. Makimura, "Layered lithium insertion material of $LiCo_{1/3}Ni_{1/3}Mn_{1/3}O_2$ for lithium-ion batteries," *Chemistry Letters*, vol. 30, no. 7, pp. 642–643, 2003.

5. Y. Terada, K. Yasaka, F. Nishikawa, T. Konishi, M. Yoshio, and I. Nakai, "In situ XAFS analysis of $Li(Mn, M)_2O_4$ (M = Cr, Co, Ni) 5V cathode materials for lithium-ion secondary batteries," *Journal of Solid State Chemistry*, vol. 156, no. 2, pp. 286–291, 2001.

6. B. Zhang, X. Wang, S. Wang, Y. Li, L. Chen, H. Jiao, Z. Yu, and J. Tu, "High-energy–density lithium manganese iron phosphate for lithium-ion batteries: Progresses, challenges, and prospects," *Journal of Energy Chemistry*, vol. 100, pp. 1–17, 2025.

7. European Union Aviation Safety Agency, *Means of Compliance with the Special Condition VTOL*, 2023. [Online]. Available: https://www.easa.europa.eu/sites/default/files/dfu/MOC-3_SC-VTOL_-_Issue_2_-_21_Jun_2023_-_FINAL.pdf. Accessed: Oct. 1, 2024.